Low-level jets and the convergence of Mars data assimilation algorithms

Todd A. Mooring[1,*], Gabrielle E. Davis[1,2], and Steven J. Greybush[3]

[1]Department of the Geophysical Sciences, University of Chicago, Chicago, Illinois, USA
[2]Department of Physics, University of Maryland, Baltimore County, Baltimore, Maryland, USA
[3]Department of Meteorology and Atmospheric Science, The Pennsylvania State University, University Park, Pennsylvania, USA
[*]Now at Department of Earth and Planetary Sciences, Harvard University, Cambridge, Massachusetts, USA

Key Points:

- Assimilating temperature data in UK-LMD Mars climate model weakens, shifts northern winter low-level jet, but has less effect on GFDL model
- Time mean flows generally agree better in the MACDA and EMARS reanalyses than in their associated control runs
- Reanalysis–control run mean state differences suggest that the EMARS control run has smaller biases than the MACDA control run

Corresponding author: Todd A. Mooring, `tmooring@alum.mit.edu`

Abstract

Data assimilation is an increasingly popular technique in Mars atmospheric science, but its effect on the mean states of the underlying atmosphere models has not been thoroughly examined. The robustness of results to the choice of model and assimilation algorithm also warrants further study. We investigate these issues using two Mars general circulation models (MGCMs), with particular emphasis on zonal wind and temperature fields. When temperature retrievals from the Mars Global Surveyor Thermal Emission Spectrometer (TES) are assimilated into the U.K.-Laboratoire de Météorologie Dynamique (UK-LMD) MGCM to create the Mars Analysis Correction Data Assimilation (MACDA) reanalysis, low-level zonal jets in the winter northern hemisphere shift equatorward and weaken relative to a free-running control simulation from the same MGCM. The Ensemble Mars Atmosphere Reanalysis System (EMARS) reanalysis, which is also based on TES temperature retrievals, also shows jet weakening (but less if any shifting) relative to a control simulation performed with the underlying Geophysical Fluid Dynamics Laboratory (GFDL) MGCM. Examining higher levels of the atmosphere, monthly mean three-dimensional temperature and zonal wind fields are in generally better agreement between the two reanalyses than between the two control simulations. In conjunction with information about the MGCMs' physical parametrizations, intercomparisons between the various reanalyses and control simulations suggest that overall the EMARS control run is plausibly less biased (relative to the true state of the Martian atmosphere) than the MACDA control run. Implications for future observational studies are discussed.

Plain Language Summary

An increasingly popular way to study Martian weather and climate is to combine atmospheric temperature observations with a computer model (specifically, a global climate model). The process of combining model and observations is called "data assimilation", and the resulting merged data set is called a "reanalysis". One advantage of reanalyses is that they include variables (such as wind) that are not directly observed. For scientific and practical applications we want these variables to be reasonably accurate—however, it is not clear how well data assimilation algorithms compute them. Our study investigates this issue using two Mars reanalyses and two model simulations that do not assimilate temperature data. We focus on slowly-varying atmospheric phenomena (timescales from 10 Mars days to a season). Assimilating temperature data into two different global climate models changes the strength and/or spatial pattern of east-west winds at low altitudes. Furthermore, monthly mean three-dimensional temperature and east-west wind fields agree better between reanalyses than between non-assimilating model simulations. This suggests that the data assimilation process is basically successful. One non-assimilating model simulation has less realistic representations of atmospheric physical processes than the other—we argue that this plausibly gives it larger biases relative to the true state of the atmosphere.

1 Introduction

Data assimilation for the Martian atmosphere has been a subject of research for more than two decades (Lewis & Read, 1995; Lewis et al., 1996; Houben, 1999) and recent years have seen a proliferation of reanalysis data sets (e.g., Montabone et al., 2014; Steele et al., 2014; Navarro et al., 2017; Holmes et al., 2018; Greybush, Kalnay, et al., 2019; Holmes et al., 2019, 2020). The Martian data assimilation problem must be solved with fewer and different observations than its terrestrial counterpart: to date, Mars reanalysis efforts have been highly dependent on infrared temperature retrievals (or at least their underlying radiances) in ways that Earth reanalyses are not (e.g., Lee et al., 2011; Montabone et al., 2014; Greybush, Kalnay, et al., 2019), (cf. Gelaro et al., 2017; Hersbach et al., 2020). This is because other dynamical information, such as surface pressure or wind observations, is available with only very limited spatial coverage (Hinson, 2008; Martínez et al., 2017).

From a dynamical perspective, atmospheric temperature structure is most clearly informative about wind fields via thermal wind or similar balance arguments (e.g., Banfield et al., 2004). However, thermal wind is at best a theory of the vertical wind shear—it cannot constrain the absolute wind at the surface and is also expected to break down in the tropics. Thus although the large-scale near-surface and tropical atmospheric circulations are basic features of the Martian climate system, it is not obvious how well they are estimated by data assimilation systems (Lewis et al., 1996, 1997; Hoffman et al., 2010). Nor are the simulations of these features by free-running Mars general circulation models (MGCMs) easy to validate.

Here we begin to address these product quality issues by investigating how assimilating temperature retrievals into MGCMs changes their climatological mean states, with particular emphasis on zonal winds. To explore the robustness of our results, we examine two different reanalyses and their associated control simulations—the control simulations differ from the reanalyses primarily by not assimilating temperature retrievals. The use of two reanalysis–control run pairs also allows us to expand on previous investigations (Waugh et al., 2016; Greybush, Gillespie, & Wilson, 2019) of whether different data assimilation systems are able to converge on a single atmospheric state. Ultimately we are able to draw some tentative conclusions about the quality of the reanalyses and control simulations, even without using any independent validation data.

The main body of this paper is divided into four major sections. We summarize the reanalysis data sets and control simulations in section 2. Results on the low-level zonal mean jets are presented in section 3, while the vertical and meridional structure of the zonal mean temperature and zonal wind fields is examined in section 4. The extent to which data assimilation converges the time mean states of the two MGCMs is addressed more formally in section 5. A summary and discussion of implications for future observational work concludes the paper, and three appendices present results of sensitivity tests and additional statistical details.

2 Reanalysis and control simulation data sets

We use the Mars Analysis Correction Data Assimilation version 1.0 (MACDA, Montabone et al., 2014) and Ensemble Mars Atmosphere Reanalysis System version 1.0 (EMARS, Greybush, Kalnay, et al., 2019) reanalyses, both of which assimilate temperature retrievals from the Mars Global Surveyor Thermal Emission Spectrometer (TES, Conrath et al., 2000). This gives the two reanalyses similar temporal extents: MY24 L_s 141° (103°) to MY27 L_s 86° (102°) for MACDA (EMARS), where the Mars years (MY) and seasonal dates are defined using the Clancy et al. (2000) calendar. However, occasional gaps in the availability of TES retrievals mean that the reanalyses are not constrained by observations throughout the full lengths of these periods. Ten intervals in which the reanalyses are thought to be poorly constrained are excluded from our study, generally following Table S1 of Mooring and Wilson (2015). (Two more such intervals occur near the beginning of the EMARS data set, but are rendered irrelevant by our choice to ignore the period prior to MY24 L_s 135°. We also do not use the MY28–33 segment of EMARS based on Mars Climate Sounder retrievals, as MACDA does not cover this period.)

The two reanalyses are underpinned by substantially different MGCMs and data assimilation algorithms. MACDA is based on the U.K.-Laboratoire de Météorologie Dynamique (UK-LMD) MGCM with a spectral dynamical core (Forget et al., 1999). The MACDA version of this model was integrated with a horizontal resolution of T31 and 25 sigma levels (Montabone et al., 2006), and the MACDA output data are available on a 5° latitude-longitude grid. EMARS uses a version of the Geophysical Fluid Dynamics Laboratory (GFDL) MGCM with a finite-volume dynamical core on a latitude-longitude grid (e.g., Hoffman et al., 2010). The horizontal resolution of this model is $\sim$5° latitude $\times$ 6° longitude, and it has 28 hybrid sigma-pressure levels.

MACDA assimilates temperature retrievals using the analysis correction method (Lewis et al., 2007), which updates the model state every dynamical timestep (480 times per sol—a sol is a Martian mean solar day, $\sim$1.03 Earth days). In contrast, EMARS assimilates temperature retrievals 24 times per sol using an ensemble Kalman filter (Hoffman et al., 2010; Zhao et al., 2015). The MACDA data set is available 12 times per sol (Montabone et al., 2014), while EMARS analyses are available 24 times per sol (Greybush, Kalnay, et al., 2019). Note that the publicly available EMARS output consists of both analyses and short (1 Mars hour) background forecasts—although many atmospheric variables are available as forecasts only, the pressure, temperature, and wind variables needed for this study are available as both analyses and forecasts and we opt to use the former as they are (slightly) more observationally constrained.

The free-running control simulations are essentially identical to their associated reanalyses, except that by definition they do not assimilate temperature retrievals. It is important to emphasize that the EMARS control simulation used in this study (version 1.02) is substantially longer than the (version 1.0) control simulation described in Greybush, Kalnay, et al. (2019), which covered only $\sim$1 Mars year of the TES era. The MACDA and EMARS control simulations will hereinafter be referred to as MCTRL and ECTRL, respectively.

Even though the control simulations are not constrained by temperature retrievals, they can still be identified with specific Mars years and seasons because their dust fields are time-dependent and constrained by observations. For MACDA and MCTRL, TES-based column opacities are assimilated using the analysis correction method (Montabone et al., 2014)—however, this particular version of the UK-LMD MGCM does not transport dust so the "forecast model" underlying the dust opacity assimilation is simply persistence. Given the analyzed column opacities, MACDA and MCTRL distribute the opacity in the vertical using a Conrath-like distribution (Conrath, 1975; Montabone et al., 2006). In contrast, the three-dimensional dust fields in EMARS and ECTRL evolve under the influences of wind advection and sedimentation (Greybush, Kalnay, et al., 2019). Agreement with observational data is maintained by nudging the column opacities towards the time-dependent dust maps of Montabone et al. (2015), which can also be considered a simple form of data assimilation. Note that the Montabone et al. (2015) dust maps for the period in question are based on retrievals not only from TES, but also from the Thermal Emission Imaging System (THEMIS) on Mars Odyssey.

3 Low-level zonal jets

We begin our comparison of the reanalysis and control run circulations by examining seasonally-resolved zonal mean zonal winds on the $\sigma = 0.991$ ($\sim$90 m above ground) level in MACDA and MCTRL. Northern (southern) winter solstice occurs at L_s 270° (90°), and focusing initially on the northern hemisphere during its local winter we see that the peak strength of the extratropical zonal jet is lower in MACDA (Figure 1a) than in MCTRL (Figure 1b). The control run jet also tends to be farther poleward than its reanalysis counterpart. This point is clarified in Figure 1c, which shows the difference between the MCTRL and MACDA fields. Figure 1c also reveals qualitatively similar behavior in the southern hemisphere near local winter solstice, which was masked in the previously mentioned figure panels by the usually weaker southern winter extratropical near-surface jet. Generally similar wind results are found on the $\sigma = 0.900$ ($\sim$1.1 km above ground) level (Appendix A, Figure A1). Furthermore, the MACDA–MCTRL jet differences are associated with differences in zonal mean surface pressure (Figure 1e). The differences in surface pressure shown in Figure 1e are qualitatively consistent with geostrophic balance and the wind differences shown in Figure 1c, although the surface geostrophic zonal wind differences are often stronger than the actual wind differences at $\sigma = 0.991$ (Figure 1d).

A comparable analysis of EMARS and ECTRL yields notably different results (Figure 2). There is a tendency for the assimilation of temperature data to weaken the extratropical winter jets near 60° latitude in both hemispheres (Figure 2a-c). However, in contrast to the situation with the UK-LMD MGCM, data assimilation has no obvious effect on the position of the zonal jets—the clear extratropical dipolar structures seen in the MACDA–MCTRL jet difference field (Figure 1c) are absent or greatly weakened in its EMARS–ECTRL counterpart (Figure 2c). The maximum magnitudes of control–reanalysis northern winter jet differences appear to be smaller for EMARS–ECTRL than for MACDA–MCTRL (Figures 1c and 2c). As with the UK-LMD MGCM, comparable results are found when winds are evaluated on a model level with $\sigma \approx 0.905$ ($\sim$1.0 km above ground, Figure A2). Interestingly, the data assimilation effect on surface pressure gradients has a different seasonality in the GFDL MGCM than in the UK-LMD MGCM—for example, the structure of the EMARS–ECTRL northern hemisphere pressure difference field (Figure 2e) changes substantially during the MY24 and MY25 L_s 225°–315° seasonal intervals but the corresponding MACDA–MCTRL field does not (Figure 1e). Furthermore, even the typical sign of the data assimilation effect on northern hemisphere summer pressure gradients differs between the GFDL and UK-LMD MGCMs (Figure 1e and 2e). However, as for MACDA–MCTRL the EMARS–ECTRL surface geostrophic wind differences (Figure 2d) effectively capture the actual patterns of low-level zonal wind differences.

Finally, we note in passing a previously undocumented and likely artificial interannual difference between MY26 and the other Mars years of EMARS. Starting near MY26 L_s $\sim$0° and continuing to L_s $\sim$105°, the zonal near-surface winds are typically westerly at the equator (Figures 2a and A2a). This is in stark contrast to the winds at this season in MY25 and MY27 of EMARS, and in all Mars years of ECTRL (Figures 2b and A2b). The abrupt transition to easterly winds near MY26 L_s 105° suggests a mechanism for this curious behavior: at approximately that time, the TES instrument was returned to its low spectral resolution (nominally 10 cm^{-1}, Conrath et al. (2000)) observing mode after having spent roughly one Mars year generally in the high spectral resolution (nominally 5 cm^{-1}) mode (Montabone et al., 2014; Holmes et al., 2020). Previous work has associated this time-dependent spectral resolution of the observations with spurious interannual variability (Wilson et al., 2014). Indeed the high-resolution observing mode received little or no use in L_s $\sim$0°–105° of the other Mars years, consistent with the idea that the anomalous MY26 L_s $\sim$0°–105° EMARS winds are a result of that period's different spectral resolution. However, further work is needed to determine how the apparent effect emerges from the assimilated temperature retrievals, which observing mode yields more realistic results, why there is no analogous effect in MACDA, and whether the abrupt cutoff of the westerlies is also influenced by a transition between EMARS production streams near MY26 L_s 105° (Greybush, Kalnay, et al., 2019).

4 Latitude-pressure structure of zonal mean fields

Unfortunately, there are very few observations directly sensitive to wind in the lower atmosphere of Mars—anemometers on a handful of landers (e.g., Martínez et al., 2017), geostrophic winds from radio occultations (e.g., Hinson et al., 1999), and arguably cloud-tracked winds from orbiter imagery (Wang & Ingersoll, 2003). The potential for a direct validation of reanalysis-based winds is thus limited. However, we can much more readily evaluate the extent to which MACDA and EMARS converge to the same solution—as they should, to the extent that the assimilated data can effectively constrain and correct biases in the MGCM states. Although our ultimate goal in this paper is to conduct a novel intercomparison of the three-dimensional time mean states of MACDA, EMARS, and their control simulations, we will lead into such an analysis with an examination of zonally-averaged time mean fields.

Because of the strong seasonality of the Martian atmosphere, for this analysis we will divide the Martian annual cycle into four seasons of nearly equal length and essentially centered on the solstices and equinoxes. More specifically, we define boreal winter, spring, summer, and autumn as L_s 216°–322°, 322°–46.7°, 46.7°–123°, and 123°–216°. The 2.5 Mars year interval from MY24 L_s 216° to MY27 L_s 46.7° then consists of exactly 10 seasons—three (two) realizations each of boreal winter and spring (summer and autumn). In Figures 1 and 2, the beginning and end of this 2.5 Mars year period are marked with solid red lines and the borders between individual seasons are marked with dashed red lines.

An initial examination of the vertical and meridional structures of zonal mean temperature and zonal wind fields suggests that assimilating TES temperature retrievals brings the UK-LMD and GFDL MGCM states closer together. Results for L_s 123°–216° and 216°–322° are shown in Figure 3. Although ECTRL is able to basically reproduce the seasonal variations seen in EMARS (black contours), the disagreements (red and blue shading) between MCTRL and ECTRL (Figure 3a, c, e, g) tend to be larger than those between MACDA and EMARS except possibly for the L_s 216°–322° zonal winds (Figure 3b, d, f, h). While MACDA is often warmer than EMARS (Figure 3b, f), maximum temperature disagreements for these seasons are larger in the free-running control simulations than in the reanalyses: for example, MCTRL can be more than 20 K warmer than ECTRL in the polar regions (Figure 3a, e). These patterns of temperature disagreement are associated with jet disagreement due to thermal wind balance—such disagreements are often but not always larger in the control simulations, especially in the extratropics for L_s 123°–216° and in high southern latitudes for L_s 216°–322° (Figure 3c, d, g, h). A tendency of temperature assimilation to converge the UK-LMD and GFDL MGCM mean states is also seen for the other two seasons (Figure 4). Although the patterns of difference between MCTRL and ECTRL are much alike in the two equinox seasons (Figures 3e, g and 4e, g), they appear to disagree more strongly during boreal summer than during boreal winter (Figures 3a, c and 4a, c).

5 Convergence of three-dimensional mean fields

We can obtain more systematic and quantitative results by computing root mean square (RMS) differences between the various free-running MGCM and reanalysis data sets. For some three-dimensional time mean field F, let us denote the (area- and mass-weighted, assuming hydrostatic balance) RMS difference between data sets X and Y as $rmsd(X, Y)$. More precisely, we define $rmsd(X, Y)$ by

$$rmsd(X,Y) = \sqrt{\frac{\int_{\phi_R} \int_0^{2\pi} \int_{p_t}^{p_b} \left(F_X - F_Y\right)^2 dp \left(\cos\phi \, d\lambda\right) \, d\phi}{\int_{\phi_R} \int_0^{2\pi} \int_{p_t}^{p_b} dp \left(\cos\phi \, d\lambda\right) \, d\phi}} \tag{1}$$

where F_X and F_Y are field F from data sets X and Y, p_t and p_b are the pressures of the top and bottom of the region of interest, and ϕ_R denotes the latitude range(s) of interest—the domain over which the meridional integral is taken need not be continuous.

It is worth explaining our definition of the time mean. Our interest is in the mean state of the atmosphere, so the averaging period must be chosen long enough to average out the transient eddies. However, an excessively long averaging period would needlessly erase information about any shorter-term changes in the mean state. We will again analyze the 2.5 Mars year interval from MY24 L_s 216° to MY27 L_s 46.7° and will attempt to balance these two competing goals by dividing each of the 10 seasons defined in section 4 into four months with approximately equal lengths of ∼41.8 sols. We then take time means over each of the 40 such months—although because we exclude periods not well constrained by TES data (section 2, Figures 1 and 2), four of these monthly means are based on less than 30 sols of data apiece. Time averaging over ∼41.8-sol months should suffice to suppress most transient eddy variability (e.g., Banfield et al., 2004; Mooring & Wilson, 2015)—to the extent that this goal is achieved, any improvement in the agreement of monthly means due to assimilation of TES temperature retrievals should come from correcting the MGCMs' time mean biases and not from synchronizing their unforced variability. Indeed, repeating the analyses with a month redefined as one-third of a season ($\sim$55.7 sols) did not qualitatively change the main results (Appendix B).

We evaluate equation 1 for each of the 40 months for two choices of F, 10 (overlapping) spatial regions of interest, and all six possible unique pairs of data sets. The fields used are temperature and zonal wind, and p_t is either 0.1 or 3 hPa. p_b is a spatially-varying monthly mean surface pressure. Specifically, for each location it is computed as the minimum of the four individual data set (MACDA, MCTRL, EMARS, ECTRL) monthly means after the data sets have all been interpolated to a single grid. The choice of $p_t = 0.1$ hPa excludes altitudes above those directly influenced by TES temperature profile assimilation (Lewis et al., 2007), while using $p_t = 3$ hPa emphasizes the lower part of the atmosphere for greater comparability to the results in section 3.

The 10 spatial regions are formed by combining the two pressure ranges with five latitude ranges: global (90°S–90°N), tropics (30°S–30°N), northern and southern hemisphere extratropics (30°–90°N and 30°–90°S, respectively) and all extratropics (the union of northern and southern extratropics). While the various latitude ranges are clearly not all independent, using multiple latitude bands is helpful for checking the robustness of the results and investigating whether the effectiveness of temperature assimilation in converging different MGCM mean states varies meridionally.

By comparing the relative sizes of the different $rmsd(X, Y)$ we provide support for two major claims:

1. Assimilating temperature retrievals into the MGCMs brings their monthly mean states into better agreement
2. ECTRL is plausibly less biased (with respect to the true monthly mean states of the Martian atmosphere) than MCTRL

Knowledge of the actual values of the $rmsd(X, Y)$ is not necessary to support these claims—instead, the results are presented in Table 1 in terms of the numbers of months (out of 40 possible) for which various inequalities involving the six $rmsd(X, Y)$ are satisfied. For compactness of notation, in these inequalities we will denote MACDA, MCTRL, EMARS, and ECTRL as M_R, M_C, E_R, and E_C, respectively.

We support the first claim by examining the inequality

$$rmsd(M_C, E_C) < rmsd(M_R, E_R) \tag{2}$$

Physically, this inequality will be satisfied if the free-running control simulations are in *better* agreement than the reanalyses are (for the given month, field, and region of interest). If this is the case, it means that assimilating TES temperature retrievals does *not* systematically bring the monthly mean states of the UK-LMD and GFDL MGCMs together—contrary to the impression created by Figures 3 and 4.

In practice, equation 2 is generally not satisfied—Table 1 indicates that equation 2 is true in at most 18 and often many fewer of the 40 total months. If consideration is restricted to the global or all-extratropics meridional regions, the inequality is satisfied for at most four months. These results strongly suggest that assimilation of the same temperature retrievals into UK-LMD and GFDL MGCM simulations tends to bring together not merely their instantaneous weather conditions, but also their climates as measured by monthly means—a more formal statistical analysis suggests that if data assimilation had no effect whatsoever on the MGCMs' monthly mean states, it is unlikely that these results would have been obtained (Appendix C). Perhaps unsurprisingly, the tendency for data assimilation to converge the monthly means appears stronger for temperature than for zonal wind—for a given region, equation 2 is always satisfied in at least as many months for zonal wind as for temperature.

We begin to support the second claim by examining

$$rmsd(M_R, M_C) < rmsd(E_R, E_C) \tag{3}$$

If satisfied, this inequality indicates that the UK-LMD reanalysis–control run pair is in better agreement than the GFDL reanalysis–control run pair. Across all of the different field–region combinations equation 3 is satisfied in as many as 26 months (Table 1). However if the tropical zonal wind cases are excluded, it is never satisfied in more than 16 months. This is evidence (albeit not always very strong) that EMARS and ECTRL are generally in better agreement than MACDA and MCTRL, at least outside the tropics. One possible explanation for this apparent result is that ECTRL is less biased (relative to the truth) than MCTRL. However, we cannot immediately dismiss the possibility that the ECTRL biases are comparable to or larger than those of MCTRL but that the EMARS ensemble Kalman filter is simply less effective than the MACDA analysis correction scheme at adjusting the mean state of a biased MGCM.

We can separate these possibilities using the additional inequalities

$$rmsd(E_R, M_C) < rmsd(E_R, E_C) \tag{4}$$

and

$$rmsd(M_R, E_C) < rmsd(M_R, M_C) \tag{5}$$

The former (latter) characterizes how well the two control simulations verify against EMARS (MACDA). If ECTRL were clearly superior to MCTRL (in the sense of verifying better against both reanalyses) then equation 5 would often be satisfied and equation 4 would not be. Likewise, if MCTRL were superior equation 4 would often be satisfied and equation 5 would not be. Alternatively, if both reanalyses were strongly biased toward their underlying MGCMs both equation 4 and equation 5 would be only rarely satisfied.

The results support the idea that ECTRL is generally less biased than MCTRL—equation 4 is satisfied in 7 months at most but equation 5 is satisfied in as many as 28 months (Table 1). Furthermore, for most field–region combinations equation 5 is satisfied in more months than equation 4—the exceptions are the tropical zonal wind cases. Statistical analysis suggests that these results—at least for the spatial regions that have $p_t = 0.1$ hPa and are not wholly tropical—are unlikely to be explicable as pure interval variability. In practice, this implies that ECTRL and MCTRL have distinct climates and are not simply different realizations of internal variability from a single climate (Appendix C). Note also that for certain field–region combinations both equation 4 and equation 5 are rarely or never satisfied, consistent with the idea that the reanalyses have some tendency to inherit the climates of their underlying MGCMs. This phenomenon is particularly prominent in the tropics.

Indeed, there are physical reasons to expect ECTRL to be less biased than MCTRL. Although both control simulations have their column dust opacities constrained to follow similar observational data sets, the constraint method used for ECTRL is more clearly consistent with the physics of dust transport in the atmosphere as described in section 2. Previous work suggests that this should yield more realistic temperatures (Wilson et al., 2008). Also, the Martian atmosphere features water ice clouds which are thought to substantially affect the thermal structure and circulation (e.g., Wilson et al., 2008; Mulholland et al., 2016). Parameterizations of the radiative effects of water ice clouds have been developed for both the GFDL and UK-LMD MGCMs (e.g., Hinson & Wilson, 2004; Mulholland et al., 2016). They are used in the EMARS–ECTRL version of the GFDL model, but not in the MACDA–MCTRL version of the UK-LMD model (Forget et al., 1999; Montabone et al., 2014; Greybush, Kalnay, et al., 2019). Since the physical parameterizations of ECTRL are a priori more realistic than those of MCTRL, it would be unsurprising if the output of the former simulation were closer to the truth.

6 Summary and discussion

We have presented a systematic intercomparison of slowly-varying components of the circulation in two Mars reanalyses and their associated free-running control simulations. The reanalyses assimilate essentially the same temperature retrievals, but via very different algorithms and into two distinct Mars general circulation models. Nevertheless, the three-dimensional monthly mean temperature and zonal wind fields are generally in better agreement for the reanalyses than for the control simulations. This suggests a certain robustness of Mars reanalyses to the choice of MGCM and assimilation algorithm, in agreement with Waugh et al. (2016) and Greybush, Gillespie, and Wilson (2019).

We devote particular attention to the low-level extratropical zonal mean zonal jets. Assimilating temperature retrievals into the UK-LMD MGCM to create MACDA tends to weaken the northern hemisphere winter jet and to shift it equatorward. Roughly similar shift behavior is found for southern hemisphere winter as well. Weakening of low-level winter jets also results when temperatures are assimilated into the GFDL MGCM, although the overall effect is more subtle than for the UK-LMD MGCM. Furthermore, changes in surface pressure gradients occur in response to temperature assimilation—these are qualitatively consistent with geostrophic balance, most evidently for northern hemisphere winter in the UK-LMD MGCM.

Finally, we have produced evidence that (at least in an average sense) the EMARS control simulation is less biased than the MACDA control simulation. Note that this result is not guaranteed to hold for individual meridional or vertical regions, such as the tropics or pressures >3 hPa—indeed, our results are consistent with the idea that the reanalyses inherit biases from their underlying MGCMs for at least some regions and fields.

Our results suggest that the low-level zonal jets of MGCMs may be biased and that similar biases might be shared across multiple MGCMs. Studies of low-level circulations in the Martian atmosphere would thus benefit from collection of additional data more sensitive to near-surface wind or pressure fields. Technological options for collecting such data include lander networks (e.g., Harri et al., 2017), radio occultation constellations (e.g., Kursinski et al., 2012), and orbiting wind lidars (e.g., Cremons et al., 2020). Alternatively, it may be possible to derive improved constraints on low-level zonal geostrophic winds from existing radio occultation and/or lander data. Further MGCM experiments and reanalysis diagnostic studies are also needed to understand the origins of the MGCM–reanalysis and inter-reanalysis disagreements documented here.

Appendix A Sensitivity of low-level jets to altitude

Our primary examination in section 3 of the seasonal and meridional variations of low-level zonal jets evaluated them on model levels roughly 0.1 km above ground (Figures 1 and 2). To make sure our findings are not strongly sensitive to this arbitrary altitude choice, we repeated the analysis on model levels roughly 1 km above ground and show the results in Figures A1 and A2. Jet behavior at the two altitudes is basically similar.

Appendix B RMS difference calculation with 30 ∼55.7-sol months

To verify that our results concerning the three-dimensional time mean states are robust to the somewhat arbitrary choice of averaging period, we repeated the root mean square (RMS) difference calculations with each of the 10 seasons divided into three months of ∼55.7 sols apiece. Tables B1 and B2 are the ∼55.7-sol month counterparts of Tables 1 and C1, respectively. While the exact quantitative results differ from those obtained with the ∼41.8-sol months, the qualitative summary text in section 5 is based on all four tables and as such is robust to the choice of a ∼41.8-sol or ∼55.7-sol averaging period.

Appendix C Statistical analyses of RMS difference results

The arguments about reanalysis convergence and the relative sizes of the MCTRL and ECTRL biases made in section 5 are based on qualitative interpretation of Tables 1 and B1 and physical reasoning. It is therefore worth investigating quantitatively how likely we are to have obtained these results under some relevant null hypotheses—could the apparent signals really just be internal variability noise?

Let us first consider the apparent convergence of the UK-LMD and GFDL Mars general circulation model (MGCM) mean states when temperature data are assimilated (Tables 1 and B1, "$rmsd(M_C, E_C) < rmsd(M_R, E_R)$" columns). We will assume (implausibly) that assimilating temperature data has no effect whatsoever on the monthly mean states of the MGCMs. If this is so, then the MACDA–EMARS RMS differences should be drawn from the same probability density functions as the MCTRL–ECTRL RMS differences and for any given month both data set pairs should have an equal probability of having the smaller RMS difference.

We will further postulate that the values of $rmsd(M_C, E_C)$ and $rmsd(M_R, E_R)$ for individual months are independent. This assumption seems reasonable, as Martian atmospheric variability that has timescales longer than our ∼41.8-sol months and that is not strongly radiatively forced by the annual cycle or via coupling to the dust field is apparently rare [e.g., *Banfield et al.*, 2004]. (The last qualifier is important because the dust fields in all four data sets are being constrained by observations and therefore we are interested only in forms of variability compatible with the prescribed dust fields.) Given this postulate, it is easy to see that (under our null hypothesis of no data assimilation effect) the number of months for which $rmsd(M_C, E_C) < rmsd(M_R, E_R)$ is satisfied is drawn from a binomial distribution with a success probability of 0.5 (Wilks, 2019a).

The probability of $rmsd(M_C, E_C) < rmsd(M_R, E_R)$ being satisfied for a number of months *less than or equal to* that actually observed is often quite small under the null hypothesis (Tables C1 and B2, "reanalyses not converging" columns). In conjunction with the physical knowledge that data assimilation does in fact affect the MACDA and EMARS states, we conclude that assimilation of temperature retrievals into the MGCMs is bringing their monthly mean states closer together. It seems unlikely that this result is solely due to data assimilation synchronizing the instantaneous weather states of models with the same underlying climate—this is because the (time-varying) weather should have been largely removed by taking the monthly means prior to computing the RMS differences. We thus conclude that data assimilation is converging distinct MGCM climates.

The first step in our argument that the EMARS control simulation is likely less biased than its MACDA counterpart is that the inequality $rmsd(M_R, M_C) < rmsd(E_R, E_C)$ is satisfied in only a minority of months for nearly all field–region combinations of interest. Next we will compute whether these results could have been obtained if $rmsd(M_R, M_C)$ and $rmsd(E_R, E_C)$ are in fact drawn from the same probability density functions—one reasonable way to operationalize the null hypothesis that MCTRL and ECTRL agree equally well with their associated reanalyses.

Our analysis of this case parallels that used to investigate whether data assimilation brings the MGCMs' mean states together. We see that under our null hypothesis that $rmsd(M_R, M_C)$ and $rmsd(E_R, E_C)$ are drawn from the same probability density functions, the number of months for which $rmsd(M_R, M_C) < rmsd(E_R, E_C)$ is satisfied is again drawn from a binomial distribution with a success probability of 0.5. Under this null hypothesis, the probability of $rmsd(M_R, M_C) < rmsd(E_R, E_C)$ being satisfied for a number of months *as or more extreme* than actually observed is often fairly low (Tables C1 and B2, "control–reanalysis differences same" columns). In other words, if there are N_{tot} months total and $rmsd(M_R, M_C) < rmsd(E_R, E_C)$ is actually satisfied in N_{obs} of them the listed value is the probability (under the null hypothesis) of it being satisfied in N months, where $0 \leq N \leq N_{obs}$ *or* $(N_{tot} - N_{obs}) \leq N \leq N_{tot}$. ($N_{tot}$ is of course 40 (30) for the ∼41.8-sol (∼55.7-sol) month case.)

We use this two-tailed statistical test because both very small *and* very large values of N_{obs} are unlikely to be observed under the stated null hypothesis. This contrasts with our use of an implicitly one-tailed test when examining whether data assimilation converges the MGCM states—a one-tailed test was appropriate in that case because satisfaction of $rmsd(M_C, E_C) < rmsd(M_R, E_R)$ in a large number of months would be inconsistent with the alternative hypothesis that data assimilation brings the MGCMs' mean states together.

The second step of our argument for smaller ECTRL biases involved comparing the rightmost two columns of Tables 1 and B1. We noted that $rmsd(M_R, E_C) < rmsd(M_R, M_C)$ was generally satisfied in at least as many months as $rmsd(E_R, M_C) < rmsd(E_R, E_C)$.

Let us define a test statistic S, where S is the number of months in which $rmsd(M_R, E_C) < rmsd(M_R, M_C)$ was satisfied minus the number of months in which $rmsd(E_R, M_C) < rmsd(E_R, E_C)$. Further denoting an observed value of S as S_{obs}, we essentially argued that ECTRL was less biased because we usually found $S_{obs} \geq 0$.

The null hypothesis we will evaluate in this case is that the ECTRL and MCTRL simulations are simply different realizations of internal variability and that these versions of the free-running GFDL and UK-LMD MGCMs actually have the same underlying climate (given the imposed dust fields). We thus postulate that the ECTRL and MCTRL monthly mean states are drawn from same (month-dependent) probability density functions, and also continue to assume that the monthly mean states for a given month are drawn independently of those for all other months.

If this null hypothesis is true, for each of the N_{tot} total months we are essentially drawing two monthly mean states from a (month-dependent) probability density function and randomly assigning the label "ECTRL" to one mean state and "MCTRL" to the other. We can thus evaluate the null hypothesis using a permutation test (Wilks, 2019b): for each of the N_{tot} months, we can independently choose to exchange (or not exchange) the "ECTRL" and "MCTRL" labels attached to the monthly mean states. There are thus $2^{N_{tot}}$ possible distinct synthetic labelings of the ECTRL and MCTRL monthly mean states. Exactly one of these labelings (the one without any exchanges) matches the actual ECTRL and MCTRL states, but if the null hypothesis is true *we are equally likely to have observed any of these labelings.*

For each field–region combination of interest, we can thus use these synthetic labelings of the monthly mean states to compute the appropriate null distribution for S. In practice, generating all $2^{N_{tot}}$ ($>10^9$ even for $N_{tot} = 30$) synthetic sets is computationally intractable—we therefore approximate the S null distribution by drawing 10^6 of the sets at random. We then calculate S_{obs} values (Tables C1 and B2, "S_{obs}" columns) and use the approximate null distributions to determine the probability of obtaining an S value *as or more extreme* than actually observed. By "as or more extreme" we mean $|S| \geq |S_{obs}|$—we are thus conducting a two-tailed test, as both large and small values of S_{obs} would argue against our chosen null hypothesis. Our results are shown in the rightmost columns of Tables C1 and B2 ("more extreme S").

Although for some field–region combinations the S_{obs} value is found to be fully consistent with the null hypothesis, in most cases with $p_t = 0.1$ hPa the probability of getting an S value at least as extreme as observed is substantially less than 1. In conjunction with the known structural differences between the two MGCMs, this finding further supports the idea that the UK-LMD and GFDL MGCMs do in fact have different climates and that the apparent superiority of ECTRL over MCTRL is not simply a random manifestation of internal variability.

Acknowledgments

We particularly thank Tiffany A. Shaw for her support of this work—she provided much helpful input on early versions of this paper and financially supported TAM and GED. R. John Wilson read drafts of the paper and pointed out the TES spectral resolution changes as the likely source of the EMARS MY26 tropical westerlies issue. Pragallva Barpanda also read an early draft of the paper. TAM was funded through Prof. Shaw's fellowship from the David and Lucile Packard Foundation, while GED was funded through National Science Foundation grant AGS-1742944 via Leadership Alliance. GED also acknowledges participation in the Leadership Alliance Summer Research Early Identification Program at the University of Chicago. SJG is supported by NASA Mars Data Analysis Program grant 80NSSC17K0690 and 80NSSC20K1054. Reduced data necessary to reproduce all figures and tables of this paper are available in Mooring et al. (2021). The full MACDA reanalysis data set is available in University of Oxford et al. (2011), while the full MACDA control simulation is available in University of Oxford et al. (2022). The full EMARS reanalysis and control simulation are available in Greybush et al. (2018).

References

Banfield, D., Conrath, B. J., Gierasch, P. J., Wilson, R. J., & Smith, M. D. (2004). Traveling waves in the Martian atmosphere from MGS TES nadir data. *Icarus*, *170*(2), 365-403. doi: 10.1016/j.icarus.2004.03.015

Clancy, R. T., Sandor, B. J., Wolff, M. J., Christensen, P. R., Smith, M. D., Pearl, J. C., ... Wilson, R. J. (2000). An intercomparison of ground-based millimeter, MGS TES, and Viking atmospheric temperature measurements: Seasonal and interannual variability of temperatures and dust loading in the global Mars atmosphere. *J. Geophys. Res.*, *105*(E4), 9553-9571. doi:

10.1029/1999JE001089

Conrath, B. J. (1975). Thermal structure of the Martian atmosphere during the dissipation of the dust storm of 1971. *Icarus*, *24*(1), 36-46. doi: 10.1016/0019-1035(75)90156-6

Conrath, B. J., Pearl, J. C., Smith, M. D., Maguire, W. C., Christensen, P. R., Dason, S., & Kaelberer, M. S. (2000). Mars Global Surveyor Thermal Emission Spectrometer (TES) observations: Atmospheric temperatures during aerobraking and science phasing. *J. Geophys. Res.*, *105*(E4), 9509-9519. doi: 10.1029/1999JE001095

Cremons, D. R., Abshire, J. B., Sun, X., Allan, G., Riris, H., Smith, M. D., ... Hovis, F. (2020). Design of a direct-detection wind and aerosol lidar for mars orbit. *CEAS Space J.*, *12*(2), 149-162. doi: 10.1007/s12567-020-00301-z

Forget, F., Hourdin, F., Fournier, R., Hourdin, C., Talagrand, O., Collins, M., ... Huot, J.-P. (1999). Improved general circulation models of the Martian atmosphere from the surface to above 80 km. *J. Geophys. Res.*, *104*(E10), 24155-24175. doi: 10.1029/1999JE001025

Gelaro, R., McCarty, W., Suárez, M. J., Todling, R., Molod, A., Takacs, L., ... Zhao, B. (2017). The Modern-Era Retrospective Analysis for Research and Applications, version 2 (MERRA-2). *J. Climate*, *30*(14), 5419-5454. doi: 10.1175/JCLI-D-16-0758.1

Greybush, S. J., Gillespie, H. E., & Wilson, R. J. (2019). Transient eddies in the TES/MCS Ensemble Mars Atmosphere Reanalysis System (EMARS). *Icarus*, *317*, 158-181. doi: 10.1016/j.icarus.2018.07.001

Greybush, S. J., Kalnay, E., Wilson, R. J., Hoffman, R. N., Nehrkorn, T., Leidner, M., ... Miyoshi, T. (2018). *The Ensemble Mars Atmosphere Reanalysis System (EMARS) version 1.0 dataset [Data set].* Penn State Data Commons. doi: 10.18113/D3W375

Greybush, S. J., Kalnay, E., Wilson, R. J., Hoffman, R. N., Nehrkorn, T., Leidner, M., ... Miyoshi, T. (2019). The Ensemble Mars Atmosphere Reanalysis System (EMARS) version 1.0. *Geosci. Data J.*, *6*(2), 137-150. doi: 10.1002/gdj3.77

Harri, A.-M., Pichkadze, K., Zeleny, L., Vazquez, L., Schmidt, W., Alexashkin, S., ... Romero, P. (2017). The MetNet vehicle: a lander to deploy environmental stations for local and global investigations of Mars. *Geoscientific Instrumentation, Methods and Data Systems*, *6*(1), 103–124. doi: 10.5194/gi-6-103-2017

Hersbach, H., Bell, B., Berrisford, P., Hirahara, S., Horányi, A., Muñoz Sabater, J., … Thépaut, J.-N. (2020). The ERA5 global reanalysis. *Q. J. Roy. Meteor. Soc.*, *146*(730), 1999-2049. doi: 10.1002/qj.3803

Hinson, D. P. (2008). *Mars Global Surveyor radio occultation profiles of the neutral atmosphere - reorganized* (Vol. USA_NASA_JPL_MORS_1101). (NASA Planetary Data System, MGS-M-RSS-5-TPS-V1.0, see figure available at `https://atmos.nmsu.edu/data_and_services/atmospheres_data/MARS/tp.html`, accessed June 18, 2019)

Hinson, D. P., Simpson, R. A., Twicken, J. D., Tyler, G. L., & Flasar, F. M. (1999). Initial results from radio occultation measurements with Mars Global Surveyor. *J. Geophys. Res.*, *104*(E11), 26997-27012. doi: 10.1029/1999JE001069

Hinson, D. P., & Wilson, R. J. (2004). Temperature inversions, thermal tides, and water ice clouds in the martian tropics. *Journal of Geophysical Research: Planets*, *109*(E1), E01002. doi: 10.1029/2003JE002129

Hoffman, M. J., Greybush, S. J., Wilson, R. J., Gyarmati, G., Hoffman, R. N., Kalnay, E., … Szunyogh, I. (2010). An ensemble Kalman filter data assimilation system for the Martian atmosphere: Implementation and simulation experiments. *Icarus*, *209*(2), 470-481. doi: 10.1016/j.icarus.2010.03.034

Holmes, J. A., Lewis, S. R., & Patel, M. R. (2020). OpenMARS: A global record of martian weather from 1999 to 2015. *Planetary and Space Science*, *188*, 104962. doi: 10.1016/j.pss.2020.104962

Holmes, J. A., Lewis, S. R., Patel, M. R., & Lefèvre, F. (2018). A reanalysis of ozone on Mars from assimilation of SPICAM observations. *Icarus*, *302*, 308 - 318. doi: 10.1016/j.icarus.2017.11.026

Holmes, J. A., Lewis, S. R., Patel, M. R., & Smith, M. D. (2019). Global analysis and forecasts of carbon monoxide on Mars. *Icarus*, *328*, 232 - 245. doi: 10.1016/j.icarus.2019.03.016

Houben, H. (1999). Assimilation of Mars Global Surveyor meteorological data. *Advances in Space Research*, *23*(11), 1899 - 1902. doi: 10.1016/S0273-1177(99)00273-2

Kursinski, E. R., McCormick, C. C., & Folkner, W. M. (2012). *An orbit-*

ing Mars atmosphere, gravity, navigation and telecommunications system. (Paper presented at Concepts and Approaches for Mars Exploration, USRA, Houston, Texas, 12–14 June, available electronically at `https://www.lpi.usra.edu/meetings/marsconcepts2012/pdf/4357.pdf`, accessed July 24, 2019)

Lee, C., Lawson, W. G., Richardson, M. I., Anderson, J. L., Collins, N., Hoar, T., & Mischna, M. (2011). Demonstration of ensemble data assimilation for Mars using DART, MarsWRF, and radiance observations from MGS TES. *Journal of Geophysical Research: Planets*, *116*(E11), E11011. doi: 10.1029/2011JE003815

Lewis, S. R., Collins, M., & Read, P. L. (1997). Data assimilation with a Martian atmospheric GCM: An example using thermal data. *Adv. Space Res.*, *19*(8), 1267-1270. doi: 10.1016/S0273-1177(97)00280-9

Lewis, S. R., & Read, P. L. (1995). An operational data assimilation scheme for the Martian atmosphere. *Adv. Space Res.*, *16*(6), 9-13. doi: 10.1016/0273-1177(95)00244-9

Lewis, S. R., Read, P. L., & Collins, M. (1996). Martian atmospheric data assimilation with a simplified general circulation model: Orbiter and lander networks. *Planet. Space Sci.*, *44*(11), 1395-1409. doi: 10.1016/S0032-0633(96)00058-X

Lewis, S. R., Read, P. L., Conrath, B. J., Pearl, J. C., & Smith, M. D. (2007). Assimilation of Thermal Emission Spectrometer atmospheric data during the Mars Global Surveyor aerobraking period. *Icarus*, *192*(2), 327-347. doi: 10.1016/j.icarus.2007.08.009

Martínez, G. M., Newman, C. N., De Vicente-Retortillo, A., Fischer, E., Renno, N. O., Richardson, M. I., ... Vasavada, A. R. (2017, Oct 01). The modern near-surface martian climate: A review of in-situ meteorological data from Viking to Curiosity. *Space Science Reviews*, *212*(1), 295–338. doi: 10.1007/s11214-017-0360-x

Montabone, L., Forget, F., Millour, E., Wilson, R. J., Lewis, S. R., Cantor, B., ... Wolff, M. J. (2015). Eight-year climatology of dust optical depth on Mars. *Icarus*, *251*, 65-95. doi: 10.1016/j.icarus.2014.12.034

Montabone, L., Lewis, S. R., Read, P. L., & Hinson, D. P. (2006). Validation of Martian meteorological data assimilation for MGS/TES using radio occultation measurements. *Icarus*, *185*(1), 113-132. doi: 10.1016/j.icarus.2006.07.012

Montabone, L., Marsh, K., Lewis, S. R., Read, P. L., Smith, M. D., Holmes, J., ... Pamment, A. (2014). The Mars Analysis Correction Data Assimilation (MACDA) dataset v1.0. *Geosci. Data J.*, *1*(2), 129-139. doi: 10.1002/gdj3.13

Mooring, T. A., Davis, G. E., & Greybush, S. J. (2021). *Data and code for Mooring, Davis and Greybush (2021, JGR-Planets), "Low-level jets and the convergence of Mars data assimilation algorithms" [Data set].* doi: 10.6082/uchicago.3421

Mooring, T. A., & Wilson, R. J. (2015). Transient eddies in the MACDA Mars reanalysis. *J. Geophys. Res.*, *120*, 1671-1696. doi: 10.1002/2015JE004824

Mulholland, D. P., Lewis, S. R., Read, P. L., Madeleine, J.-B., & Forget, F. (2016). The solsticial pause on Mars: 2 modelling and investigation of causes. *Icarus*, *264*, 465-477. doi: 10.1016/j.icarus.2015.08.038

Navarro, T., Forget, F., Millour, E., Greybush, S. J., Kalnay, E., & Miyoshi, T. (2017). The challenge of atmospheric data assimilation on Mars. *Earth and Space Science*, *4*(12), 690-722. doi: 10.1002/2017EA000274

Steele, L. J., Lewis, S. R., Patel, M. R., Montmessin, F., Forget, F., & Smith, M. D. (2014). The seasonal cycle of water vapour on Mars from assimilation of Thermal Emission Spectrometer data. *Icarus*, *237*, 97 - 115. doi: 10.1016/j.icarus.2014.04.017

University of Oxford, The Open University, Montabone, L., Lewis, S. R., & Read, P. L. (2011). *Mars Analysis Correction Data Assimilation (MACDA): MGS/TES v1.0 [Data set].* NERC EDS Centre for Environmental Data Analysis. doi: 10.5285/78114093-E2BD-4601-8AE5-3551E62AEF2B

University of Oxford, The Open University, Montabone, L., Lewis, S. R., & Read, P. L. (2022). *Mars Analysis Correction Data Assimilation (MACDA): MGS/TES v1.0 Reference Run Data [Provisional data set].* NERC EDS Centre for Environmental Data Analysis. (Available electronically at `https://catalogue.ceda.ac.uk/uuid/acdfa050673c46d49d6a35bfa482762b`.)

Wang, H., & Ingersoll, A. P. (2003). Cloud-tracked winds for the first Mars Global Surveyor mapping year. *Journal of Geophysical Research: Planets*, *108*(E9). doi: 10.1029/2003JE002107

Waugh, D. W., Toigo, A. D., Guzewich, S. D., Greybush, S. J., Wilson, R. J., & Montabone, L. (2016). Martian polar vortices: Comparison of reanalyses. *Journal of Geophysical Research: Planets*, *121*(9), 1770-1785. doi: 10.1002/2016JE005093

Wilks, D. S. (2019a). Chapter 4 - parametric probability distributions. In *Statistical methods in the atmospheric sciences* (Fourth ed., p. 77-141). Elsevier. doi: 10.1016/B978-0-12-815823-4.00004-3

Wilks, D. S. (2019b). Chapter 5 - frequentist statistical inference. In *Statistical methods in the atmospheric sciences* (Fourth ed., p. 143-207). Elsevier. doi: 10.1016/B978-0-12-815823-4.00005-5

Wilson, R. J., Greybush, S. J., McConnochie, T. H., & Kass, D. (2014). *Assessment of seasonal and interannual variability in TES and MCS observations.* (Paper presented at Eighth International Conference on Mars, USRA, Pasadena, California, 14–18 July, available electronically at `http://www.hou.usra.edu/meetings/8thmars2014/pdf/1468.pdf`, accessed October 27, 2021)

Wilson, R. J., Lewis, S. R., Montabone, L., & Smith, M. D. (2008). Influence of water ice clouds on Martian tropical atmospheric temperatures. *Geophys. Res. Lett.*, *35*(7), L07202. doi: 10.1029/2007GL032405

Zhao, Y., Greybush, S. J., Wilson, R. J., Hoffman, R. N., & Kalnay, E. (2015). Impact of assimilation window length on diurnal features in a Mars atmospheric analysis. *Tellus A*, *67*, 26042. doi: 10.3402/tellusa.v67.26042

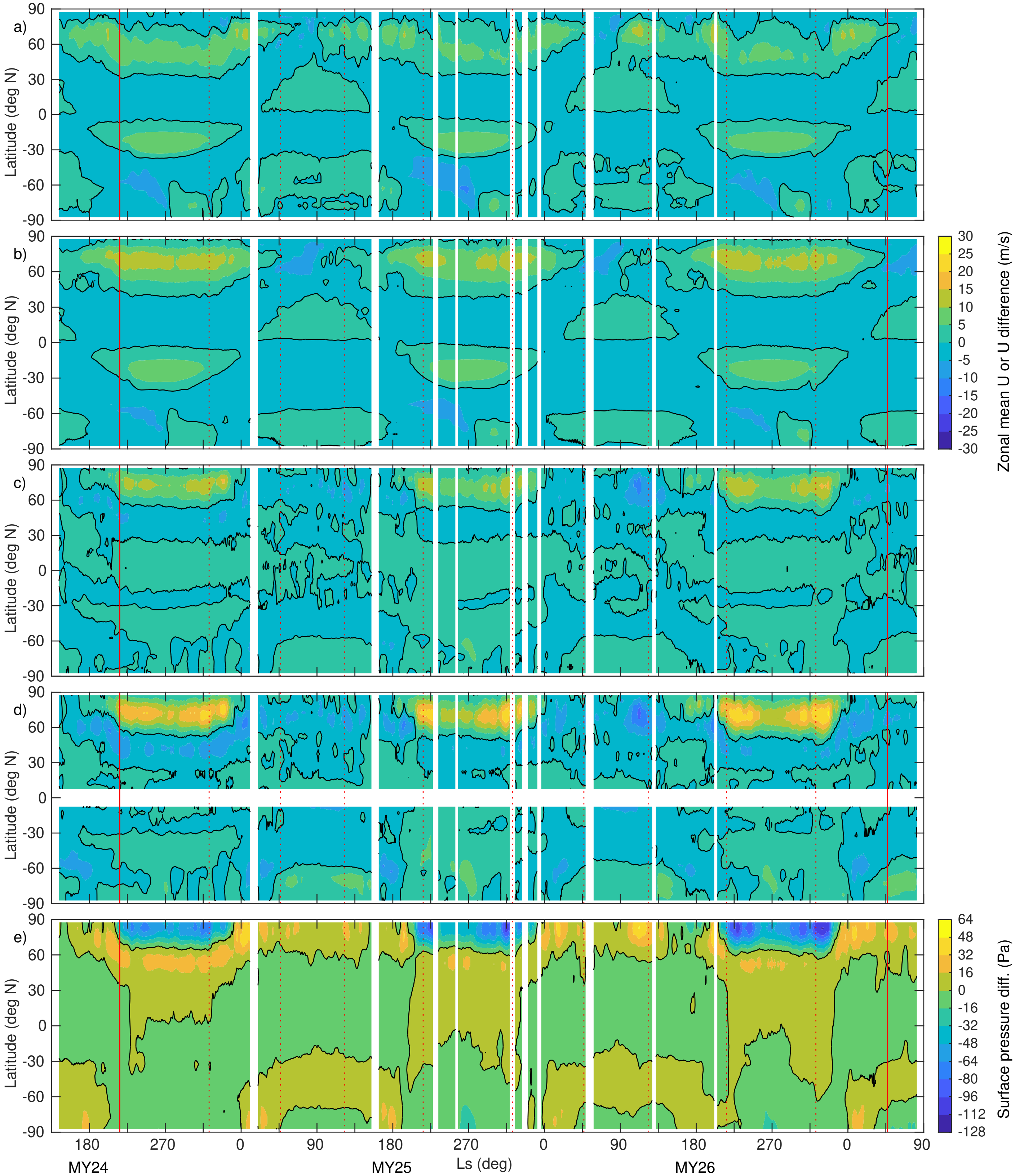

Figure 1. Zonal mean zonal winds on the $\sigma = 0.991$ level (∼90 m above ground) for MACDA (a) and MCTRL (b). Differences between MCTRL and MACDA are shown in (c-e)— $\sigma = 0.991$ zonal winds in (c), surface geostrophic zonal winds in (d) and surface pressures in (e). The time range shown is MY24 L_s 135° to MY27 L_s 90°. All fields have been smoothed with a 10-sol running mean. The surface geostrophic wind difference in (d) was computed from surface pressure and temperature data from the lowest model level, following equation 4 of Mooring and Wilson (2015). (Geostrophic wind differences are not plotted within 7.5° of the equator.) The global mean atmospheric mass difference at each timestep was removed before plotting (e). The black line is the zero contour, notable gaps in the availability of TES retrievals are masked out in white, and the limits of the seasons used in Figures 3 and 4 are marked with red lines.

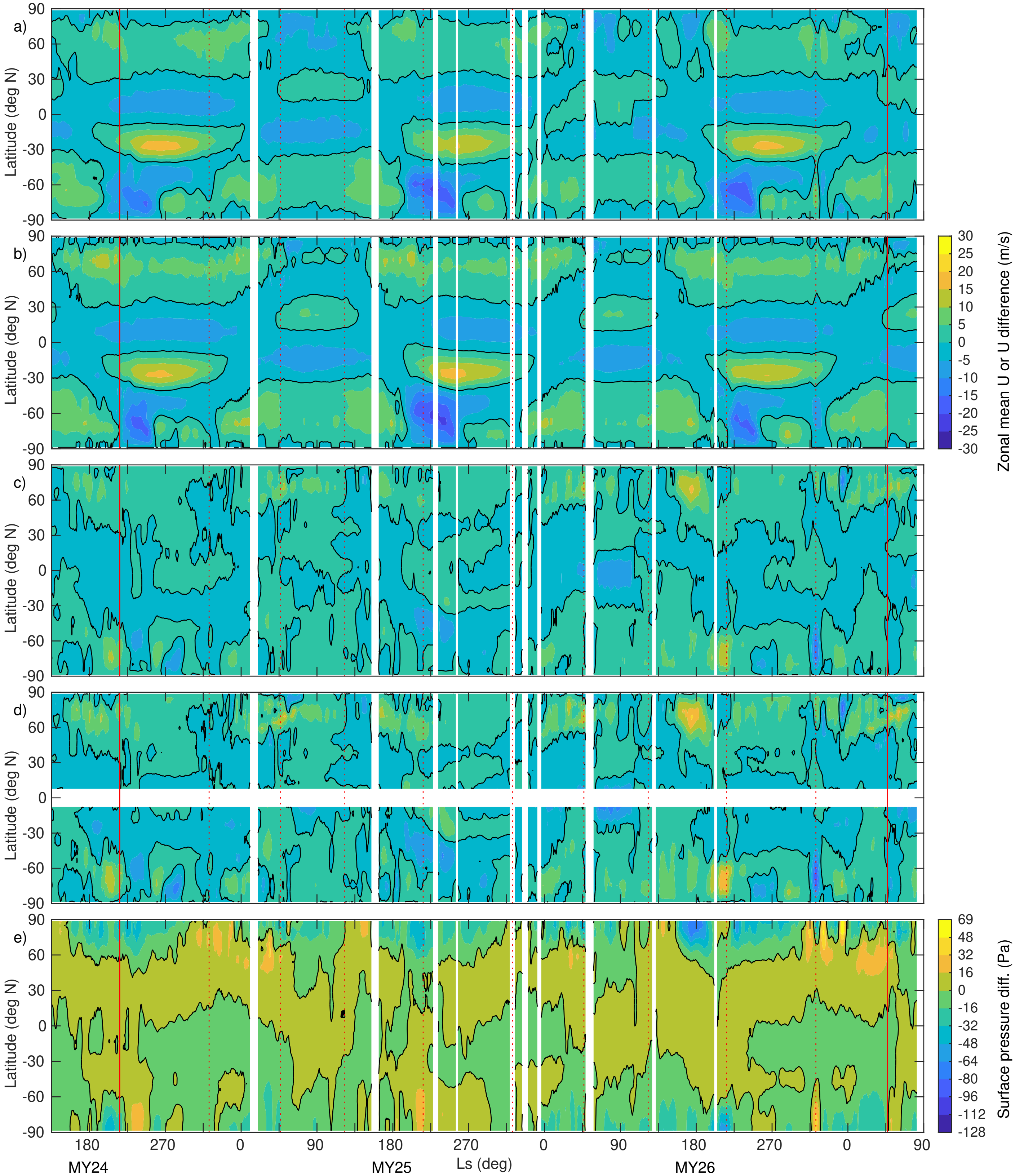

Figure 2. As Figure 1 but for EMARS and ECTRL. Zonal winds in (a-c) are evaluated on the model level with $\sigma \approx 0.988$ ($\sim$120 m above ground).

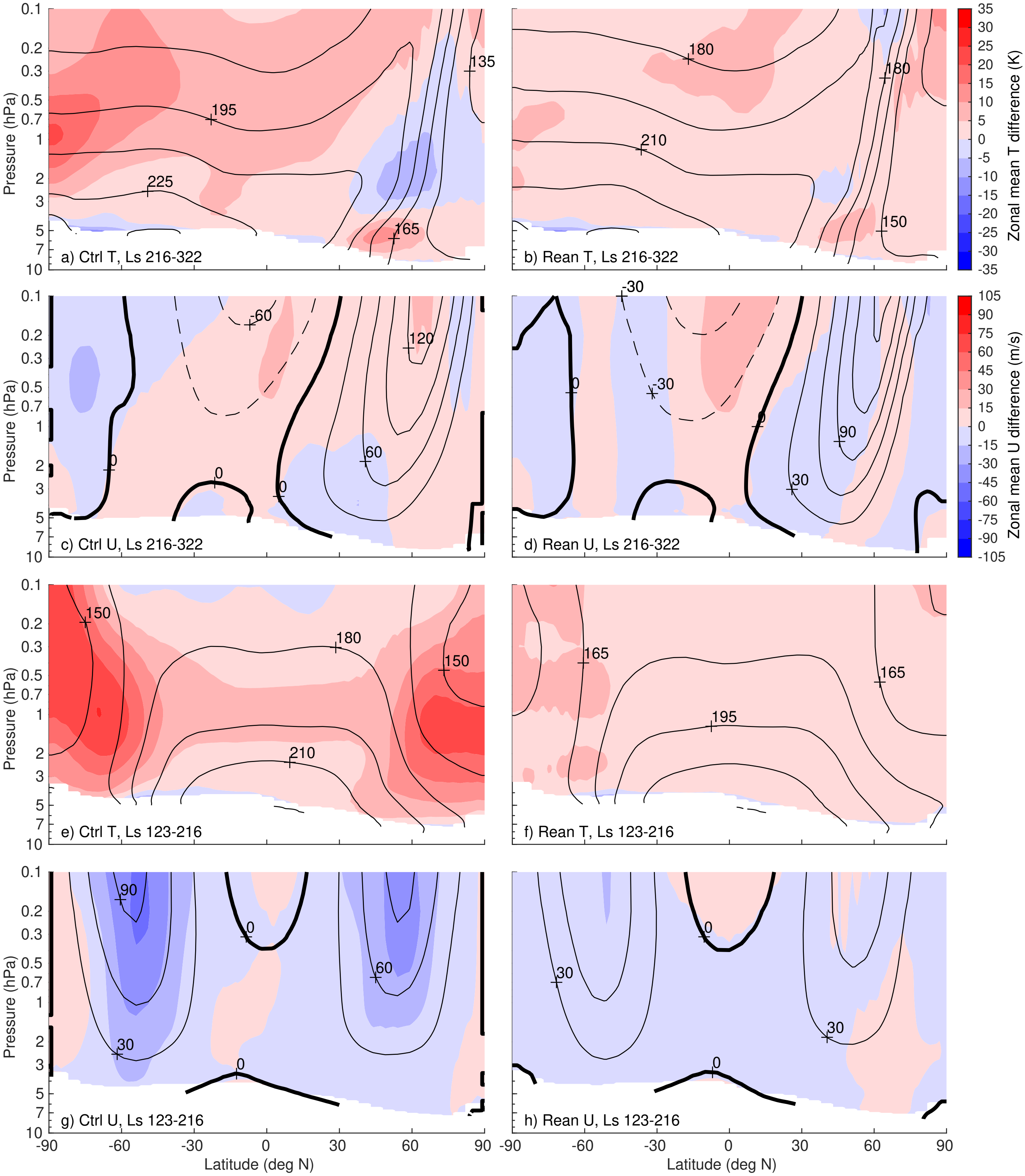

Figure 3. Agreement between reanalysis and free-running control zonal mean temperature and zonal wind fields for boreal winter (a-d) and autumn (e-h). Black contours in the left (right) column show full fields from ECTRL (EMARS), with the zero contour marked with a heavy black line. Red and blue shading in the left (right) column shows MCTRL minus ECTRL (MACDA minus EMARS). Interannual means are computed across all available realizations of each season, while each single-Mars year seasonal mean is computed from four monthly means. The months have lengths of ~41.8 sols, as described in section 5.

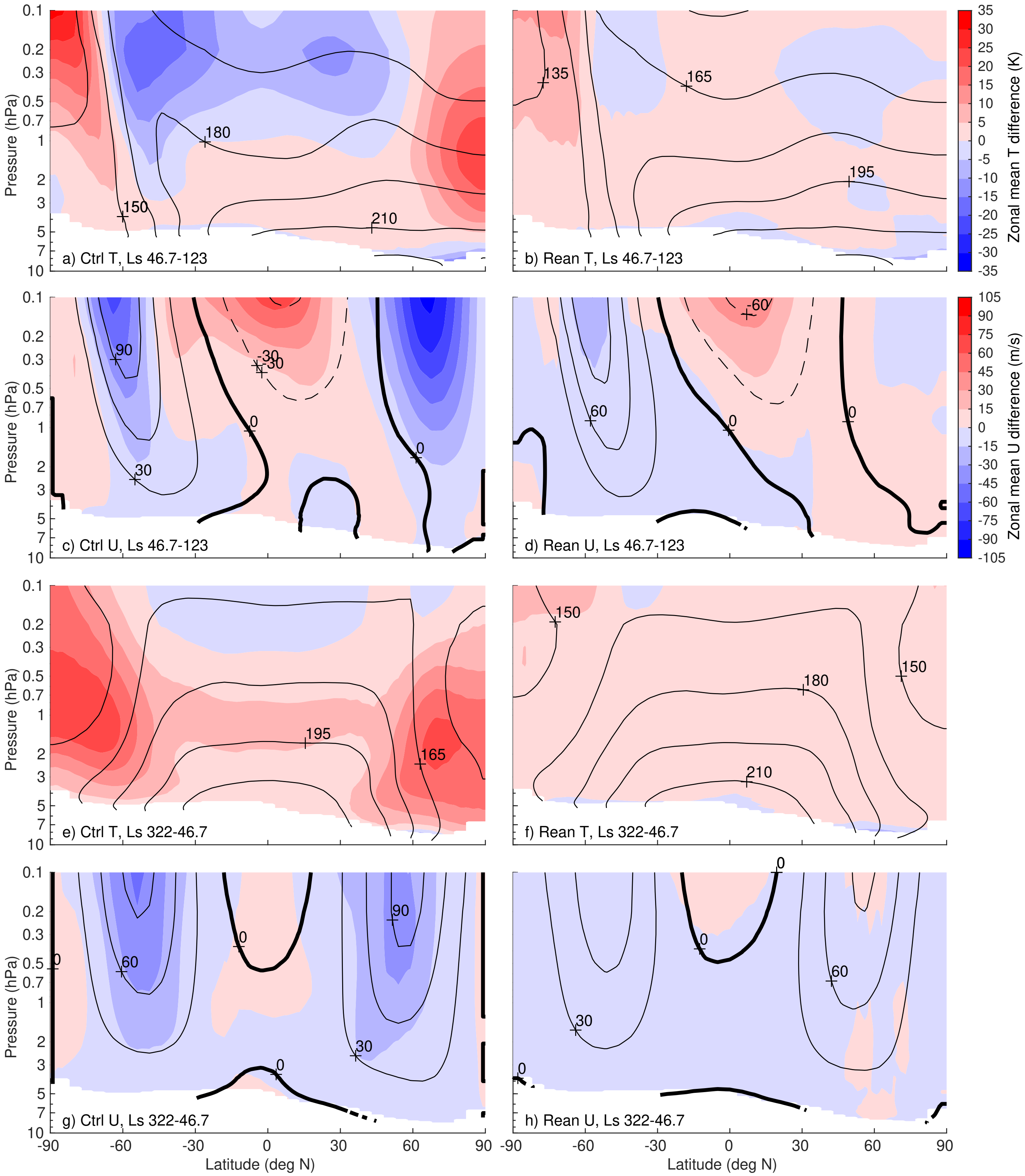

Figure 4. As Figure 3, but for boreal summer (a-d) and spring (e-h).

Table 1. Relative sizes of RMS differences between reanalyses and control simulations

Field	Domain top (hPa)	Meridional domain	$rmsd(M_C, E_C) < rmsd(M_R, E_R)$	$rmsd(M_R, M_C) < rmsd(E_R, E_C)$	$rmsd(E_R, M_C) < rmsd(E_R, E_C)$	$rmsd(M_R, E_C) < rmsd(M_R, M_C)$
T	0.1	Global		7		14
T	0.1	Tropics	1	5		6
T	0.1	SH extratropics		12	2	11
T	0.1	NH extratropics		12	7	24
T	0.1	All extratropics		8	3	18
T	3	Global		11	2	7
T	3	Tropics	3	4		3
T	3	SH extratropics	5	12	3	8
T	3	NH extratropics		15	6	15
T	3	All extratropics		12	3	7
U	0.1	Global	1	10		19
U	0.1	Tropics	17	18		
U	0.1	SH extratropics	8	6	1	14
U	0.1	NH extratropics	1	9	6	28
U	0.1	All extratropics		4		28
U	3	Global	4	16	2	13
U	3	Tropics	18	26	5	
U	3	SH extratropics	13	11	3	4
U	3	NH extratropics	8	11	6	20
U	3	All extratropics	2	11	1	15

This table contains information about relative levels of agreement between the various reanalysis and control simulation data sets. We denote the RMS difference between data sets X and Y as $rmsd(X, Y)$. The left three columns name the variable being analyzed and the region over which RMS differences are being computed. The right four columns contain the results, expressed as the number of months (of 40 total) for which the inequality given at the top of each column is satisfied. Zeros have been omitted for clarity. As an example of how to read the table, the large number of values $\ll$40 in the $rmsd(E_R, M_C) < rmsd(E_R, E_C)$ column means that EMARS is in robustly better agreement with ECTRL than with MCTRL.

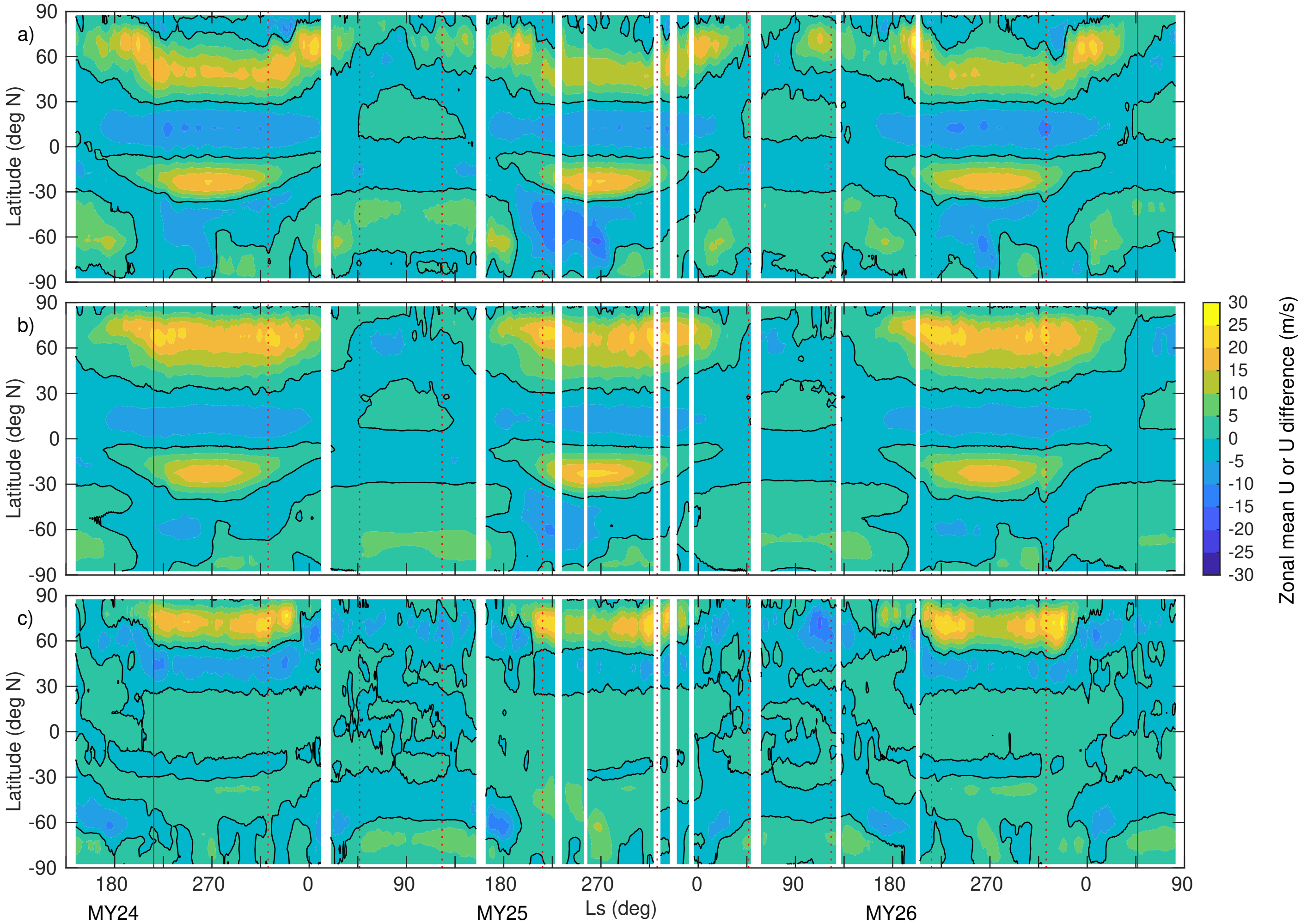

Figure A1. As Figure 1a-c, but for the $\sigma = 0.900$ level (~1.1 km above ground).

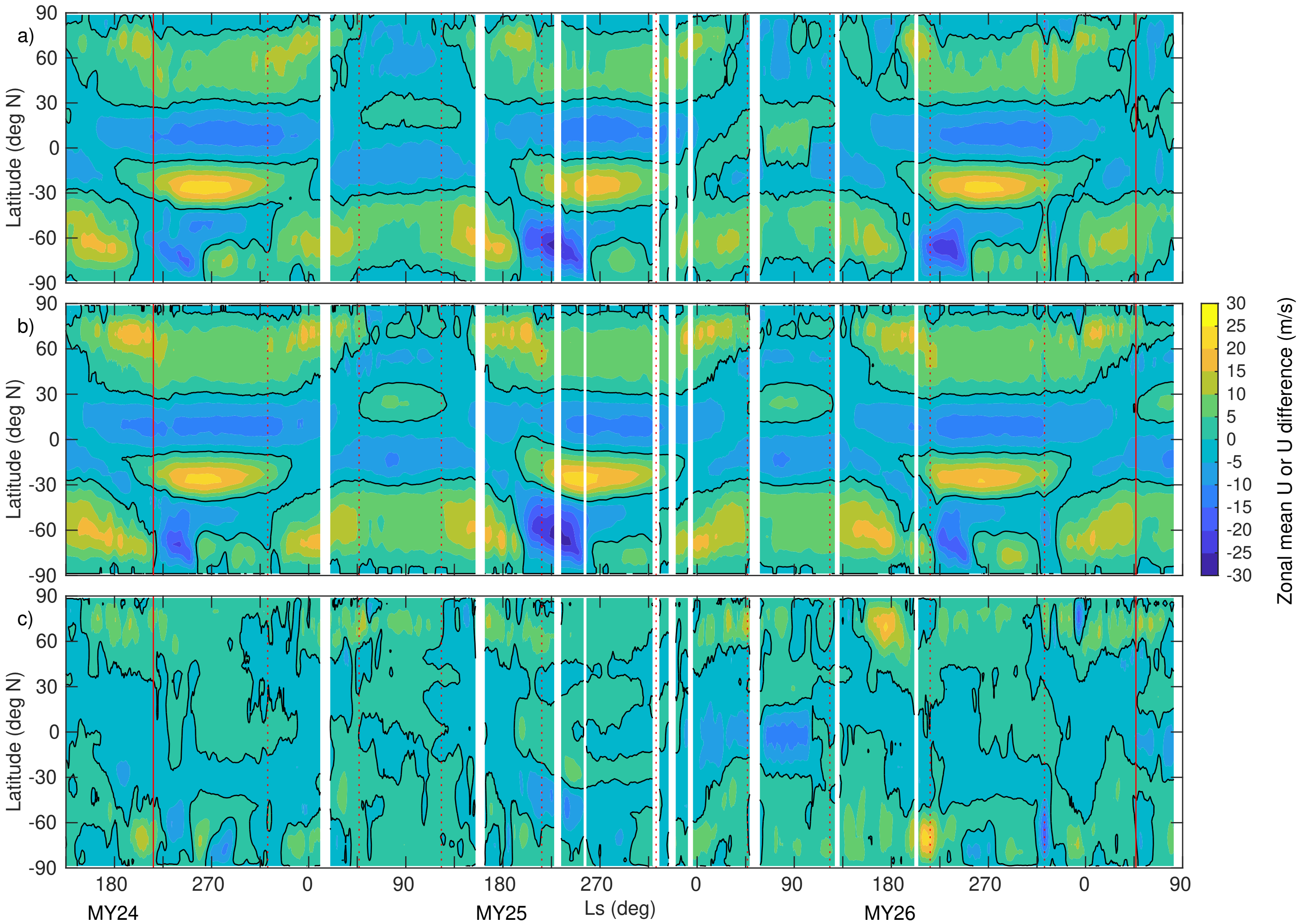

Figure A2. As Figure 2a-c, but on the model level with $\sigma \approx 0.905$ (~1.0 km above ground).

Table B1. Relative sizes of RMS differences between reanalyses and control simulations

Field	Domain top (hPa)	Meridional domain	$rmsd(M_C, E_C) <$ $rmsd(M_R, E_R)$	$rmsd(M_R, M_C) <$ $rmsd(E_R, E_C)$	$rmsd(E_R, M_C) <$ $rmsd(E_R, E_C)$	$rmsd(M_R, E_C) <$ $rmsd(M_R, M_C)$
T	0.1	Global		5		12
T	0.1	Tropics	1	3		5
T	0.1	SH extratropics		7	1	8
T	0.1	NH extratropics		11	5	17
T	0.1	All extratropics		8	3	14
T	3	Global		7		6
T	3	Tropics	2	1		2
T	3	SH extratropics	4	9	2	7
T	3	NH extratropics		10	7	10
T	3	All extratropics		8		7
U	0.1	Global	1	5		15
U	0.1	Tropics	14	13		
U	0.1	SH extratropics	5	3	1	12
U	0.1	NH extratropics		6	5	22
U	0.1	All extratropics		3	1	20
U	3	Global	4	10	1	8
U	3	Tropics	14	20	3	
U	3	SH extratropics	11	7	3	4
U	3	NH extratropics	6	7	4	16
U	3	All extratropics	2	7		12

As Table 1, but using 30 ∼55.7-sol months instead of 40 ∼41.8-sol months.

Table B2. Information about probabilities of obtaining the observed results under various null hypotheses

Field	Domain top (hPa)	Meridional domain	Reanalyses not converging	Control–reanalysis differences same	S_{obs}	More extreme S
T	0.1	Global	$\mathbf{9.31 \times 10^{-10}}$	*3.25×10^{-4}*	12	*4.44×10^{-4}*
T	0.1	Tropics	$\mathbf{2.89 \times 10^{-8}}$	$\mathbf{8.43 \times 10^{-6}}$	5	6.24×10^{-2}
T	0.1	SH extratropics	$\mathbf{9.31 \times 10^{-10}}$	*5.22×10^{-3}*	7	3.89×10^{-2}
T	0.1	NH extratropics	$\mathbf{9.31 \times 10^{-10}}$	2.00×10^{-1}	12	1.69×10^{-2}
T	0.1	All extratropics	$\mathbf{9.31 \times 10^{-10}}$	1.61×10^{-2}	11	1.25×10^{-2}
T	3	Global	$\mathbf{9.31 \times 10^{-10}}$	*5.22×10^{-3}*	6	3.14×10^{-2}
T	3	Tropics	$\mathbf{4.34 \times 10^{-7}}$	$\mathbf{5.77 \times 10^{-8}}$	2	5.00×10^{-1}
T	3	SH extratropics	$\mathbf{2.97 \times 10^{-5}}$	4.28×10^{-2}	5	1.80×10^{-1}
T	3	NH extratropics	$\mathbf{9.31 \times 10^{-10}}$	9.87×10^{-2}	3	6.30×10^{-1}
T	3	All extratropics	$\mathbf{9.31 \times 10^{-10}}$	1.61×10^{-2}	7	1.56×10^{-2}
U	0.1	Global	$\mathbf{2.89 \times 10^{-8}}$	*3.25×10^{-4}*	15	$\mathbf{5.90 \times 10^{-5}}$
U	0.1	Tropics	4.28×10^{-1}	5.85×10^{-1}	0	1
U	0.1	SH extratropics	*1.62×10^{-4}*	$\mathbf{8.43 \times 10^{-6}}$	11	*3.45×10^{-3}*
U	0.1	NH extratropics	$\mathbf{9.31 \times 10^{-10}}$	*1.43×10^{-3}*	17	*4.31×10^{-4}*
U	0.1	All extratropics	$\mathbf{9.31 \times 10^{-10}}$	$\mathbf{8.43 \times 10^{-6}}$	19	$\mathbf{1.70 \times 10^{-5}}$
U	3	Global	$\mathbf{2.97 \times 10^{-5}}$	9.87×10^{-2}	7	3.95×10^{-2}
U	3	Tropics	4.28×10^{-1}	9.87×10^{-2}	-3	2.50×10^{-1}
U	3	SH extratropics	1.00×10^{-1}	*5.22×10^{-3}*	1	1
U	3	NH extratropics	*7.15×10^{-4}*	*5.22×10^{-3}*	12	1.17×10^{-2}
U	3	All extratropics	$\mathbf{4.34 \times 10^{-7}}$	*5.22×10^{-3}*	12	*5.07×10^{-4}*

As Table C1, but using 30 ∼55.7-sol months.

This table should be used to help

interpret the results given in Table B1.

Table C1. Information about probabilities of obtaining the observed results under various null hypotheses

Field	Domain top (hPa)	Meridional domain	Reanalyses not converging	Control–reanalysis differences same	S_{obs}	More extreme S
T	0.1	Global	$\mathbf{9.09 \times 10^{-13}}$	$\mathbf{4.23 \times 10^{-5}}$	14	$\mathit{1.14 \times 10^{-4}}$
T	0.1	Tropics	$\mathbf{3.73 \times 10^{-11}}$	$\mathbf{1.38 \times 10^{-6}}$	6	3.13×10^{-2}
T	0.1	SH extratropics	$\mathbf{9.09 \times 10^{-13}}$	1.66×10^{-2}	9	2.26×10^{-2}
T	0.1	NH extratropics	$\mathbf{9.09 \times 10^{-13}}$	1.66×10^{-2}	17	$\mathit{3.32 \times 10^{-3}}$
T	0.1	All extratropics	$\mathbf{9.09 \times 10^{-13}}$	$\mathit{1.82 \times 10^{-4}}$	15	$\mathit{1.46 \times 10^{-3}}$
T	3	Global	$\mathbf{9.09 \times 10^{-13}}$	$\mathit{6.43 \times 10^{-3}}$	5	1.80×10^{-1}
T	3	Tropics	$\mathbf{9.73 \times 10^{-9}}$	$\mathbf{1.86 \times 10^{-7}}$	3	2.50×10^{-1}
T	3	SH extratropics	$\mathbf{6.91 \times 10^{-7}}$	1.66×10^{-2}	5	2.27×10^{-1}
T	3	NH extratropics	$\mathbf{9.09 \times 10^{-13}}$	1.54×10^{-1}	9	7.87×10^{-2}
T	3	All extratropics	$\mathbf{9.09 \times 10^{-13}}$	1.66×10^{-2}	4	3.44×10^{-1}
U	0.1	Global	$\mathbf{3.73 \times 10^{-11}}$	$\mathit{2.22 \times 10^{-3}}$	19	$\mathbf{3.00 \times 10^{-6}}$
U	0.1	Tropics	2.15×10^{-1}	6.36×10^{-1}	0	1
U	0.1	SH extratropics	$\mathbf{9.11 \times 10^{-5}}$	$\mathbf{8.36 \times 10^{-6}}$	13	$\mathit{1.02 \times 10^{-3}}$
U	0.1	NH extratropics	$\mathbf{3.73 \times 10^{-11}}$	$\mathit{6.80 \times 10^{-4}}$	22	$\mathit{1.82 \times 10^{-4}}$
U	0.1	All extratropics	$\mathbf{9.09 \times 10^{-13}}$	$\mathbf{1.86 \times 10^{-7}}$	28	**0**
U	3	Global	$\mathbf{9.29 \times 10^{-8}}$	2.68×10^{-1}	11	$\mathit{7.55 \times 10^{-3}}$
U	3	Tropics	3.18×10^{-1}	8.07×10^{-2}	-5	6.27×10^{-2}
U	3	SH extratropics	1.92×10^{-2}	$\mathit{6.43 \times 10^{-3}}$	1	1
U	3	NH extratropics	$\mathbf{9.11 \times 10^{-5}}$	$\mathit{6.43 \times 10^{-3}}$	14	$\mathit{9.19 \times 10^{-3}}$
U	3	All extratropics	$\mathbf{7.47 \times 10^{-10}}$	$\mathit{6.43 \times 10^{-3}}$	14	$\mathit{5.36 \times 10^{-4}}$

See text of Appendix C for further details, including descriptions of the columns. Calculations were done using 40 ~41.8-sol months, and thus this table should be used to help interpret the results given in Table 1. Probabilities $< 10^{-4}$ are written in **bold**, while probabilities $< 10^{-2}$ are *italicized*.